extruded into the ice or possibly underwater before the development of the WAIS.

Other satellite imagery over the ice streams and their catchment basins suggests that the volcano we have identified is not an isolated feature beneath the WAIS. Strikingly circular features in the Landsat images from ice stream E in West Antarctica[15] might also be interpreted as volcanic constructs. The main implication of active volcanism beneath the ice is that elevated geothermal flux provides an important control on the dynamics of the WAIS. Spatial variations in geothermal flux will regulate the water supply available for saturating the sediment responsible for ice streaming. If the rifting process is providing the melt water and sediment required for ice streaming, then the ice streams may be unable to migrate beyond the edge of the active portion of the West Antarctic rift system. This edge would be a major geological boundary between thin hot actively extending lithosphere and cold inactive lithosphere. We believe such a boundary exists between the lithosphere of the interior Ross embayment, the relatively flat low-lying area between Marie Byrd Land and the Transantarctic Mountains, and the region dominated by the Ellsworth–Whitmore crustal block and the Byrd subglacial basin[16]. If the downstream terminus of the ice streams were to retreat to this geological boundary, then the reservoir of slow-moving inland ice would be exposed to the ocean without the buffer of the ice-stream system; this would almost certainly represent an unstable situation. Therefore, the character of the lithosphere within the central West Antarctic rift system and, specifically, the distribution of elevated heat flow and sedimentary basins, represents a fixed boundary condition for the WAIS that is independent of global climate yet could be responsible for triggering the collapse of the ice sheet. □

Received 22 October 1992; accepted 5 January 1993.

1. Mercer, J. H. *Nature* **271,** 321–325 (1978).
2. Thomas, R. H. *J. Glaciol.* **24,** 167–177 (1979).
3. MacAyeal, D. R. *Nature* **359,** 29–32 (1992).
4. Blankenship, D. D., Bentley, C. R., Rooney, S. T. & Alley, R. B. *Nature* **322,** 54–57 (1986).
5. Alley, R. B., Blankenship, D. D., Bentley, C. R. & Rooney, S. T. *Nature* **332,** 57–59 (1986).
6. LeMasurier, W. E. *Abstr. Progr.* **10,** 443 (Geological Society of America, 1978).
7. Wilson, T. J., *Antarct. J.* **25,** 31–34 (1991).
8. Davey, F. J. in *The Antarctic Continental Margin: Geology and Geophysics of the Western Ross Sea,* 1–16 (Circum-Pacific Council for Energy and Resources, Houston, 1987).
9. Behrendt, J. C., Cooper, A. K. & Yuan, A. in *The Antarctic Continental Margin: Geology and Geophysics of the Western Ross Sea,* 155–177 (Circum-Pacific Council for Energy and Resources, Houston, 1987).
10. LeMasurier, W. E. & Thomson, J. W. (eds) *Volcanoes of the Antarctic Plate and Southern Oceans* (American Geophysical Union, 1990).
11. Robin, G. de Q. *Nature* **215,** 1029–1032 (1967).
12. Paterson, W. S. B. *The Physics of Glaciers* (Pergamon, Oxford, 1981).
13. Bjornsson, H. *Jökull* **33,** 13–18 (1983).
14. Clarke, G. K. C., Cross, G. M. & Benson, C. S. *J. geophys. Res.* **94,** 7237–7249 (1989).
15. Bindschadler, R. A. & Scambos, T. A. *Science* **252,** 242–246 (1991).
16. Dalziel, I. W. D. & Elliot, D. H. *Tectonics* **1,** 3–19 (1982).
17. Drewry, D. J. *Antarctica: Glaciological and Geophysical Folio* (Scott Polar Research Institute, Cambridge, 1983).

ACKNOWLEDGEMENTS. We thank K. Najmulski, K. Griffiths, M. Noonan, V. Childers, J. Jarvis, S. Dopplehammer, R. Arko, M. Peters, K. Killilea, J. Peryea, R. Campbell and the personnel of Ken Borek Air Ltd. for their long-term technical support. The work was improved by helpful comments from I. W. D. Dalziel, R. B. Alley, and D. R. MacAyeal. This work was supported by the Division of Polar Programs of the U.S. NSF.

Seismological mapping of fine structure near the base of the Earth's mantle

John E. Vidale & Harley M. Benz

United States Geological Survey, 345 Middlefield Road, Menlo Park, California 94025, USA

THE Earth's core–mantle boundary (CMB) juxtaposes liquid iron and crystalline silicates, and is a region of large vertical thermal gradients. The D″ region, which extends up to 200–300 km above the CMB, often has elevated shear-wave velocity and suggestions of lateral variations in structure[1]. Recent improvements in our ability to assemble and analyse records from regional seismic networks have allowed us to examine long profiles of travel times, amplitudes and waveforms from more than a thousand short-period seismometers[2]. We observe, across Canada and the United States, P waves that have grazed the CMB from the powerful nuclear test in Lop Nor, China, on 21 May 1992. First-arrival travel times and large secondary arrivals are consistent with a 1.5% compressional velocity increase with depth ~130 km above the CMB—about half the thickness of D″ in this locality[3]. Our observations, together with evidence for the absence of such a thin, fast layer in neighbouring regions, suggest the presence of lateral heterogeneity in composition or phase at the base of the mantle.

Discrimination between the various thermal and compositional explanations of heterogeneity at the base of the mantle requires knowledge of variations in the velocity of both compressional (P) and shear (S) waves. The D″ layer is laterally heterogeneous[1,4–8]: some studies find a sudden increase with depth in the P- and S-wave velocities 200–300 km above the CMB[1,6–11], whereas others infer smoother velocity variations[6,12]. A P-wave velocity decrease in the deepest 100 km of the mantle has also been inferred[10,13,14], suggesting a thermal boundary layer[15,16].

The nuclear explosion at Lop Nor, China, with a yield of 0.66 Mt (megatonnes high explosive equivalent) (21 May 1992, 41.55° N 88.84° E, 1.6 km deep, $m_b = 6.5$; L. Gao and T. C. Wallace, personal communication), provided a large, impulsive P-wave source. It has been more than 10 years since the last explosions of this size, and the seismic networks at that date were much more sparse. The size of the Lop Nor explosion allows us to see short-period P waves diffracting into the distances of the core shadow, and its brief duration allows us easily to isolate multiple arrivals separated by only 1–2 s. By assembling many records from a single event, we avoid the problem faced by previous researchers of how to combine records of an array of events, with generally unknown origin-time errors, mislocations and amplitude calibration between events.

We use the digital short-period seismograms from 14 regional networks in the United States and Canada[17] to investigate the structure above the CMB. The P waves graze the core between the sections of the CMB beneath northern Alaska and Greenland (Fig. 1). The 477 seismograms with the lowest background and signal-generated noise levels were chosen from a total of 1,062 available.

Figure 2 shows seismic sections of stations in three narrow azimuthal ranges. The P wave is simple in the range from 80° to 92°. Later arrivals appear in the distance range from 92° to 103°, which vary in timing and amplitude with azimuth from the explosion. A clear arrival with slightly smaller amplitude follows the P wave by 1–3 s in each profile. Much less distinct later arrivals are seen for profiles across the eastern third of North America. This secondary arrival is not due to scattering near the receivers, as it is absent in earthquakes that we have examined and it is similar for nearby stations. It does not arise from source complexity, as it is absent in the distance range from 80° to 92°.

The secondary arrival is travelling 0.25 s deg^{-1} more slowly than the initial P arrival. Figure 3*a* presents the first and secondary arrival times. The pattern is typical of an abrupt increase in velocity with depth: the slowness (reciprocal apparent velocity) of the first arrival decreases abruptly from 5.0 s deg^{-1} in the

distance range 80° to 90° to 4.5 s deg^{-1} in the distance range 90° to 103°.

Ray tracing and reflectivity modelling verify that this arrival can be explained as a wide-angle reflection from a thin, fast layer at the base of the mantle. The reflections from the core (PcP) and from the top of the layer should be too small to be observed. The secondary arrival's slowness at the surface in a radial velocity structure would be r_r/r_0v_r, whereas the core-grazing P wave has the slowness r_b/r_0v_b. v_r is the velocity just above the reflector, v_b is the velocity just above the CMB, r_0 is the radius of the Earth, r_r is the radius to the reflector and r_b is the radius of the core. The difference in slowness between the wave grazing the top of the thin layer and the wave grazing the CMB is $\Delta v r_b/v_b^2$ plus $\Delta r/v_b$, where Δv is the velocity contrast across the top of the thin layer and Δr the thickness of the layer, in the limit of small thickness and velocity contrast.

We estimate that two-thirds of the difference in slowness between the two arrivals is caused by the difference between r_r and r_b with the following argument. If the refracting layer is 130 km thick, then the layer is 1.5% faster than the mantle just above. A smaller velocity contrast and thicker layer would not produce the 6–10° range of observation of the secondary arrival. A larger velocity contrast across the refracting interface would require a thinner layer, but the thickness of 130 km is consistent with the time difference between the arrivals and the cross-over of the two phases near 89°.

The strength and coherence of arrivals shown in Fig. 2 suggest that a single interface is the primary structure. Some energy that corresponds to the wide-angle reflection from roughly 250 km above the CMB, perhaps the top of D″, appears 4–10 s behind the diffracted P wave in the distance range from 93° to 98°, but this observation is much less clear. The large amplitude of the secondary arrival would be difficult to produce by scattering from low-contrast structures of dimension less than the 300-km path on the CMB sampled by this study. Weak layering is the most likely explanation for the secondary arrival in Figs 2 and 3. The measurement of a significantly larger thickness for D″, 200–300 km, in the region that we sample[3] suggests that we are observing an additional layer. The 1,500-km Fresnel zone of the long-period shear waves that image the top of D″ (ref. 3) leaves open the possibility of a local depression in the top of D″ to 130 km above the CMB; however, the paucity of wide-angle P-wave reflections that would indicate normal D″ thickness across our large array, argues against this explanation.

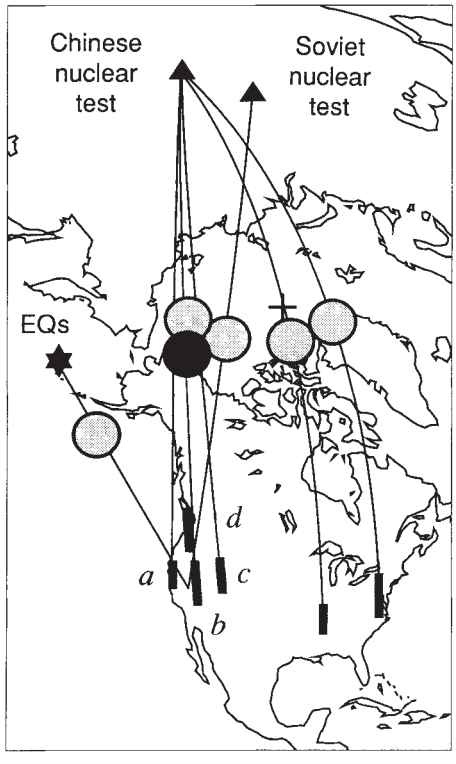

FIG. 1 The great circle paths of the rays sampling the CMB from nuclear tests in China and the Soviet Union and earthquakes in the Andreanof Islands. The heavy lines labelled *a*, *b*, *c* and *d* correspond to the profiles shown in Fig. 2. The dark region shows a 130-km-thick layer at the base of the mantle, the light regions do not show such a structure. The size of the circles, a few hundred kilometres, roughly indicates the areas of the core–mantle boundary sampled. The resolution is difficult to specify, as it depends on unresolved details of the structure.

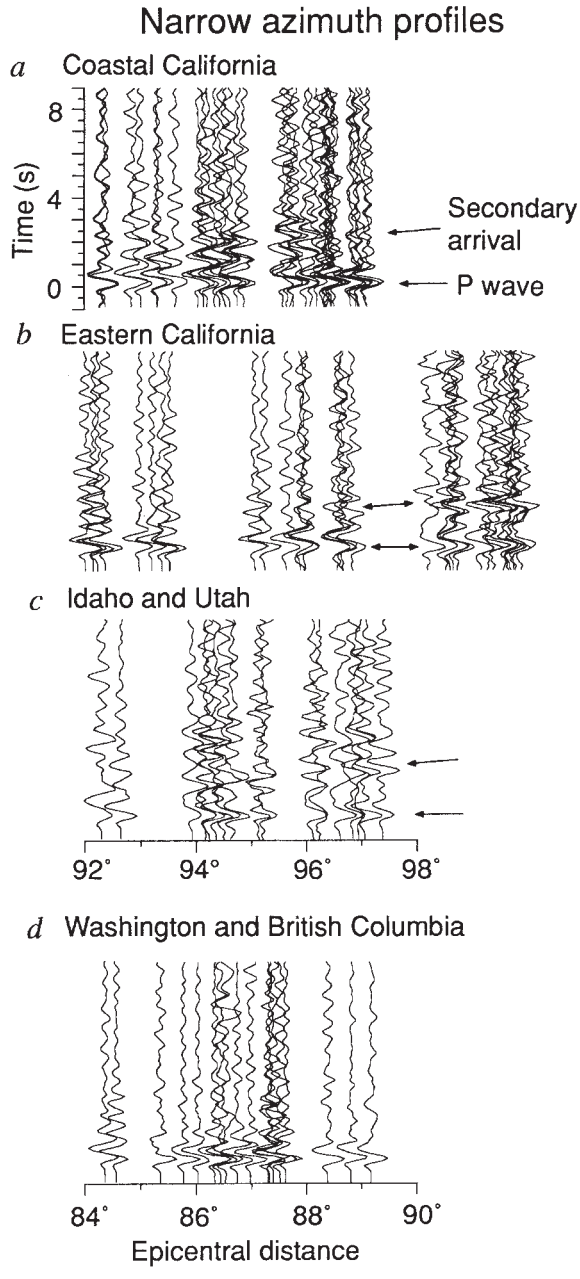

FIG. 2 Seismogram record sections from the Chinese nuclear test. The seismograms have been aligned so that the initial P waves arrive simultaneously and are plotted trace-normalized. The waveforms include the instrument response. First, sections for narrow source-to-receiver azimuthal ranges are shown for the distance range 92° to 100°. *a*, The 36 receivers with azimuths between 24.1° and 24.5°. *b*, The 32 receivers with azimuths between 22° and 23°. *c*, The 17 receivers between 15.7° and 16.5°. *d*, The 18 receivers for the distance range 84° to 90° between the azimuths 20° and 20.5°.

An irregular structure is suggested by the variations in amplitude and timing of the secondary arrival. The arrival varies in amplitude and distance range of observability across North America (Fig. 2) and is absent for some of the stations in Nevada between profiles *b* and *c* that are not shown. The arrival is roughly 0.5 s earlier to the west (azimuths 24° to 25°, Fig. 2*a*) than to the east (azimuths 15.5° to 17°, Fig. 2*c*). This difference corresponds to variation of 15–30 km in the reflector depth across a span of 250 km at the CMB. Irregularity or lateral intermittence is also suggested by the lack of secondary near-critical reflections in the distance range 80° to 90°, because for radial layering, such arrivals would accompany the observed wide-angle reflections. It is possible, however, that irregularity in boundary depth or seismic velocities above the boundary would disrupt the near-critical reflection more than the wide-angle reflection.

The CMB has a thermal boundary layer (TBL) with a temperature contrast of 800–2,000 K (refs 16, 18). The TBL does not explain our observation, because it would lead to a slower layer at the base of the mantle, rather than the observed faster layer. The low P velocity of a TBL would affect the amplitude and timing more than the waveform of the diffracted P waves. Figure 4 shows an estimate of the amplitude of the P wave for stations near the west coast of the United States. The amplitude decay with distance is simple, without the fluctuations and diminished rate of decay predicted by numerical calculations for reduced velocity TBL structures[6]. It is therefore unlikely that our inference of a fast layer is complicated by the presence of a strong velocity gradient due to the TBL.

Several nearby areas do not show such a layer. Records of the Chinese explosion from eastern North America do not show the distinct layer arrival visible in the west. A large-aperture array study of core reflections from earthquakes beneath the Andreanof Islands[2] found no suggestion of short-period S-to-P conversions greater than 0.5% in or above D″ in a location about 1,500 km from the current study region. No secondary arrival or kink in the travel times as a function of distance is seen across the Washington and Northern California seismic networks from a Soviet test (50° N, 42° E, 17 December 1988). Finally, the lack of a secondary arrival closer than the distance of the travel-time kink in Fig. 3 suggests that the layering is also less pronounced at distances slightly closer to the Chinese explosion. These areas are shown in Fig. 1.

A fast layer 160–200 km thick has previously been inferred beneath the northern Soviet Union, Indonesia and the Caribbean from P-wave travel times and waveforms in the distance range from 75° to 92° (refs 8–10). These observations, although limited in array aperture and clarity of the secondary arrival, show similar features. The lowermost mantle beneath northern Alaska, where we find the fast layer, is also known to be much faster than average from tomographic studies of long-period shear waves (G. Masters, personal communication).

The factors that perturb the shear and compressional wave velocities in the lowermost mantle are not well known; nor is the relation between D″ and the thinner anomaly seen above with compressional waves. The phase transition from sodium chloride to caesium chloride structure in oxides[20] and a phase transition in the stishovite component[21] have been proposed as possible explanations of D″ structure, but the pressures of these hypothesized transitions have not been measured precisely enough to require their occurrence within the D″ layer. Anisotropy caused by shearing within a boundary layer at the base of the mantle is also a possibility.

A layer that is 25% enriched in stishovite relative to the overlying mantle and 130 km thick can explain our observations. Reactions between the core and mantle[22,23] may be important in generating a stishovite-enriched layer. Such a layer would be 1–2% fast for P waves, and consistent with the timing, amplitude and distance range of the triplication that we observe. It may be less anomalous for S waves[20], explaining the absence of all but subtle S-wave wide-angle reflections[7]. Finally, the small

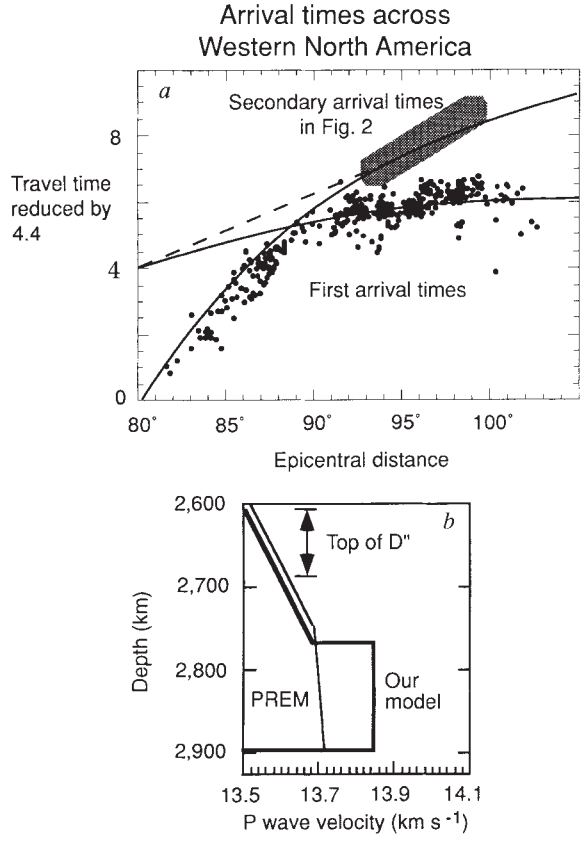

FIG. 3 *a*, Travel times from the Chinese nuclear test to stations in the azimuth range from 0° to 30°, which spans the western United States. The shaded region indicates approximate arrival times of the secondary arrivals identified in Fig. 2. The light line indicates the arrival times predicted by our velocity model (*b*), which is compared with the reference model PREM[25].

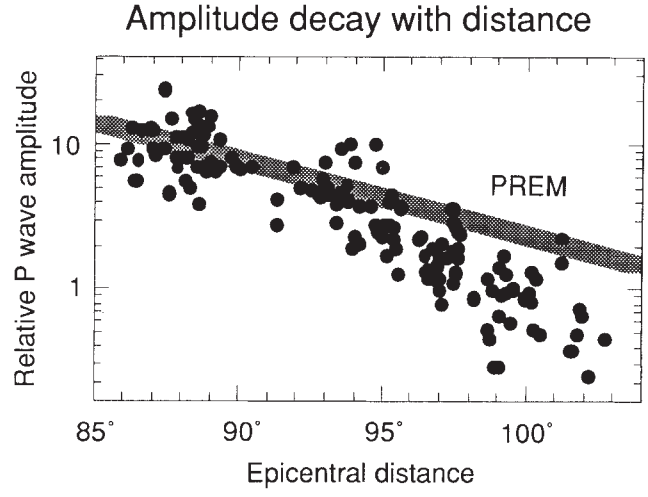

FIG. 4 The amplitude of the P arrival across the Washington, Northern California, and Southern California seismic arrays, expressed as the ratio relative to the ScP arrival from the 13 March 1992 Andreanof earthquake[26]. ScP is expected to show slightly increasing amplitude with distance, so the P amplitudes probably decrease more rapidly with distance than shown. The ratio minimizes scatter due to near-surface impedance contrasts and focusing. The light line shows an amplitude decay curve calculated for the reference model PREM[6,25].

contrast density and, possibly, S-wave velocity or the intermittent presence of the layer would explain the lack of long-period S-wave near-vertical reflections[24]. □

Received 7 September 1992; accepted 5 January 1993.

1. Lay, T. *Eos* **70,** 49–59, 1989.
2. Vidale, J. E. & Benz, H. M. *Nature* **359,** 627–629 (1992).
3. Young, C. J. & Lay, T. *J. geophys. Res.* **95,** 17385–17402 (1990).
4. S. M. Flatté & Wu, R. S. *J. geophys. Res.* **93,** 6601–6615 (1988).
5. Wysession, M. E., Okal, E. A. & Bina, C. R. *J. geophys. Res.* **97,** 8749–8764, (1992).
6. Young, C. J. & Lay, T. *Phys. Earth Planet. Inter.* **54,** 64–81 (1989).
7. Gaherty, J. B. & Lay, T. *J. geophys. Res.* **97**, 417–435 (1992).
8. Weber, M. & Davis, J. P. *Geophys. J. int.* **102,** 231–256 (1990).
9. Ruff, L. J. & Helmberger, D. V. *Geophys. J. R. astr. Soc.* **68,** 95–119 (1982).
10. Wright, C., Muirhead, K. J. & Dixon, A. E. *J. geophys. Res.* **90,** 623–634 (1985).
11. Baumgardt, D. R. *Geophys. Res. Lett.* **16,** 657–660 (1989).
12. Schlittenhardt, J. *J. geophys.* **60,** 1–18 (1986).
13. Cleary, J. R. *Phys. Earch planet. Inter.* **30,** 13–27 (1974).
14. Doornbos, D. J. *J. geophys. Res.* **88,** 3498–3505 (1983).
15. Jeanloz, R. & Richter, F. M. *J. geophys. Res.* **84,** 5497–5504 (1979).
16. Williams, Q. & Jeanloz, R. *J. geophys. Res.* **95,** 19299–19310 (1990).
17. Benz, H. M., Vidale, J. E. & Mori, J. *Eos* (submitted).
18. Boehler, R., von Bargen, N., & Chopelas, A. *J. geophys. Res.* **95,** 21731–21737 (1990).
19. Wright, C. & Lyons, J. A. *Pure appl. Geophys.* **119,** 137–162 (1981).
20. Jeanloz, R. & Thompson, A. B. *Rev. Geophys. Space Phys.* **21,** 51 (1983).
21. Tsuchida, Y. & Yagi, T. *Nature* **340,** 217–220 (1989).
22. Knittle, E. & Jeanloz, R. *Science* **251,** 1438–1443 (1989).
23. Ruff, L. J. & Anderson, D. L. *Phys. Earth planet. Inter.* **21**, 181–201 (1980).
24. Revenaugh, J. & Jordan, T. H. *J. geophys. Res.* **96,** 19811–19824 (1991).
25. Dziewonski, A. M. & Anderson, D. L. *Phys. Earth planet. Inter.* **25,** 297–356 (1982).
26. Vidale, J. E. & Benz, H. M. *Nature* **359,** 627–629 (1992).

ACKNOWLEDGEMENTS. We thank Q. Williams, S. Grand and T. Lay for discussions, the University of California at Santa Cruz deep Earth scientists for comments and M. Weber, J. Schweitzer, F. Krüger and M. Wysession for reviews. The cooperation of the short-period networks in North America has been essential to the success of this effort.

Haldane's rule has multiple genetic causes

H. Allen Orr

Center for Population Biology, University of California, Davis, California 95616, USA

HALDANE'S rule states that "When in the F_1 offspring of two different animal races one sex is absent, rare, or sterile, that sex is the heterozygous [heterogametic or XY] sex"[1]. This rule represents one of the few patterns characterizing animal speciation[2,3]. Traditional explanations of Haldane's rule[1,4–6] claim that heterogametic hybrids are unfit because they lack an X chromosome that is 'compatible' with the autosomes of one species. Recent work[2,7] shows that this explanation is incorrect for hybrid sterility: contrary to prediction, homogametic hybrids carrying both X chromosomes from the same species remain fertile. Until now, similar tests have not been performed for hybrid inviability. Here I show that homogametic hybrids who carry both X chromosomes from the same species are inviable. These results show that the genetic causes of Haldane's rule differ for hybrid sterility versus inviability. Haldane's rule does not, therefore, have a single genetic basis.

The cross of *Drosophila simulans* females to *D. teissieri* males obeys Haldane's rule: only hybrid females appear[8] (Table 1). Hybrid males (the heterogametic sex in *Drosophila*) die during the first or second larval instar. The traditional Haldane–Dobzhansky–Muller[1,4–6] explanation of Haldane's rule claims that these males are inviable because they are genetically 'unbalanced': they lack some X-linked gene product from *D. teissieri* required by the *D. teissieri* autosomes to produce fit adults. Perhaps the strongest test of this theory involves producing hybrid *females* who carry both X chromosomes from the same species and a haploid set of autosomes from each species (Fig. 1). Because these 'unbalanced' female hybrids also lack an X chromosome from one species they should also be unfit[7]. Although repeated tests have disproved this explanation of Haldane's rule for hybrid sterility—unbalanced females remain fertile[2]—this simple test has not been performed for cases of Haldane's rule for inviability owing to the unavailability of the required genetic stocks.

As an attached-X chromosome (C(1)RM) is available in *D. simulans*, I was able to perform this critical test in the *D. simulans*–*D. teissieri* hybridization: the *D. simulans* C(1)RM female X *D. teissieri* male hybridization produces hybrid females who are just as genetically unbalanced as the inviable F_1 hybrid males. These females carry two *D. simulans* X chromosomes, a haploid set of autosomes from each species, a Y from *D. teisseri*, and cytoplasm from *D. simulans*, just as do the inviable F_1 males. As Table 1 shows, the results of this test are simple: no C(1)RM adult hybrid females ever appeared. Unbalanced females are, therefore, lethal. Sexing of hybrid larvae and pupae revealed that these females die in the same developmental stage as F_1 $X_{simulans}/Y_{teissieri}$ males (first or second larval instar).

The inviability of these females strongly suggests that the genetic basis of Haldane's rule differs for hybrid sterility and hybrid inviability. To test this possibility further, I did a similar analysis in a second hybridization. The *D. melanogaster* female X *D. simulans* male hybridization yields only females, whereas the reciprocal cross reportedly yields many males with a few rare females[9–11], that is, this direction of the cross is reportedly an exception to Haldane's rule. As such, this hybridization has been considered an inappropriate place to test the basis of Haldane's rule (if F_1 females are already inviable, the interpretation of any inviability of 'unbalanced' females is obviously muddied). However, we have recently discovered that many, if not all, extant strains of these species yield abundant hybrid females in both directions of the species cross, at least at lower temperatures (18°–22 °C) (see Table 1 for details). The *D. melanogaster*–*D. simulans* hybridization clearly obeys Haldane's rule.

This species pair thus affords another opportunity to test the basis of Haldane's rule for inviability. Although unbalanced hybrid females from this cross (carrying an attached X from *D. melanogaster*) have been repeatedly described as inviable[11,12],

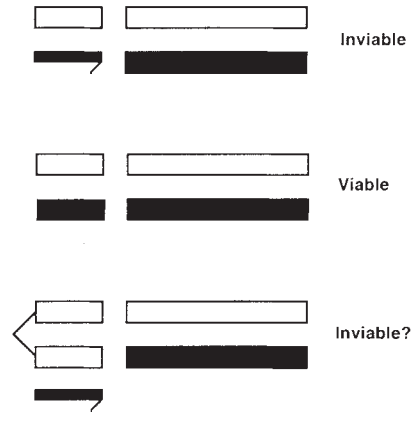

FIG. 1 Test of the genetic basis of Haldane's rule. The chromosomes of one species (for example, *D. simulans*) are shown in white and those of the other species (for example, *D. teissieri*) in black. Sex chromosomes are shown at the left (X on top; Y, with 'hook', on the bottom). Haploid sets of autosomes shown at the right. All genotypes carry cytoplasm from the 'white' species. The top genotype represents F_1 male hybrids and the middle genotype represents F_1 female hybrids. The bottom genotype depicts hybrid females who carry an attached X chromosome from the 'white' species. The traditional explanation of Haldane's rule predicts that this 'unbalanced' genotype will be inviable. (Population genetic models (H.A.O., unpublished) show that this theory requires an additional assumption: the alleles causing reproductive isolation act as loss-of-function mutations; that is more recessive alleles must have greater homozygous effects on hybrid fitness.)